Observation of Cluster Size Growth in CO-Directed Synthesis of Au-25(SR)(18) Nanoclusters

ARTICLE *in* ACS NANO · AUGUST 2012

Impact Factor: 12.88 · DOI: 10.1021/nn3023206 · Source: PubMed

5 AUTHORS, INCLUDING:

Yong Yu
Agency for Science, Technology and Researc…
23 PUBLICATIONS **626** CITATIONS
SEE PROFILE

Yue Yu
National University of Singapore
18 PUBLICATIONS **771** CITATIONS
SEE PROFILE

Jim Yang Lee
National University of Singapore
315 PUBLICATIONS **16,499** CITATIONS
SEE PROFILE

Jianping Xie
National University of Singapore
110 PUBLICATIONS **4,402** CITATIONS
SEE PROFILE

Observation of Cluster Size Growth in CO-Directed Synthesis of $Au_{25}(SR)_{18}$ Nanoclusters

Yong Yu, Zhentao Luo, Yue Yu, Jim Yang Lee,* and Jianping Xie*

Department of Chemical and Biomolecular Engineering, National University of Singapore, 10 Kent Ridge Crescent, Singapore 119260

ABSTRACT

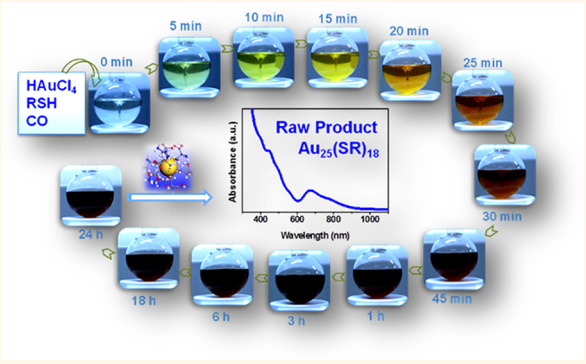

The design of an efficient synthesis for large-scale production of atomically precise nanoclusters (NCs) is pivotal in realizing the size-dependent properties of the NCs. A simple and versatile method for producing atomically precise thiolated gold NCs ($Au_{25}(SR)_{18}$ NCs) in large quantities (~200 mg) is demonstrated in this study. It uses a gaseous reducing agent, carbon monoxide (CO), to support a slow and size-controlled growth of $Au_{25}(SR)_{18}$ NCs. Absorption measurements of the reaction solution, which underwent distinct color changes (colorless → yellow → orange → brown → red-brown), allowed the formation of thiolated Au_{25} NCs to be reconstructed from several key intermediates. The unique reaction environment provided by gaseous CO presents a new synthetic route to fabricate atomically precise metal NCs in quantities large enough for application explorations.

KEYWORDS: gold nanoclusters · ultrasmall nanoparticles · monodisperse · carbon monoxide · optical absorption

Thiolated Au nanoclusters (NCs) are a family of ultrasmall (<2 nm) particles stabilized by thiol ligands.[1,2] They have become a most important type of nanoparticles in recent years owing to their unique molecular-like properties, such as quantized charging[3−5] and luminescence.[6−9] Due to the strong quantum confinement effect in this size regime, the physical and chemical properties of NCs are mainly governed by the particle size.[1,10] The large-scale production of thiolated Au NCs in well-controlled sizes (or atomically precise NCs) is therefore a most pivotal step toward utilizing their size-tunable properties (*e.g.,* catalytic[11−13] and optical[14]).

Thiolated Au NCs are generally synthesized *via* the reductive decomposition of thiolate-Au(I) complexes by a strong reducing agent (*e.g.,* sodium borohydride, $NaBH_4$).[15−17] The fast reduction kinetics often leads to the formation of a mixture of thiolated Au NCs in different sizes. A high-resolution separation technique (*e.g.,* polyacylamide gel electrophoresis (PAGE) and size-exclusion chromatography (SEC)) is therefore required to isolate thiolated Au NCs of a particular size.[18−21] For example, an early successful preparation of atomically precise thiolated Au NCs (10.4 kDa species) reported by the Whetten group was based on a PAGE separation.[20] This Au NC species was later identified as $Au_{25}(SR)_{18}$ by electrospray ionization mass spectrometry (ESI-MS).[14] $Au_{25}(SR)_{18}$ NCs are extremely stable even under harsh reaction conditions, such as in the presence of excess thiol ligands.[22] Recently, several thermodynamic selection (or size focusing) methods have been used to synthesize $Au_{25}(SR)_{18}$ NCs,[22−24] and their molecular structure has also been resolved.[25,26] The other two successful syntheses of atomically precise thiolated Au NCs were Au_{38} and Au_{144}, which also displayed excellent stability.[27−31] The synthesis of thiolated Au NCs in other sizes is less attempted probably because of their lower stability.[22,32] More recently, several kinetic control methods have also been developed and demonstrated for a discrete number of thiolated Au NCs, such as Au_{19}, Au_{20}, and Au_{24}.[33−35] Many of these methods, however, are constrained by relatively complicated procedures, long synthesis time, or difficulties in large-scale production.[24,28,29,36] There is evidently a need for facile and scalable methods for the preparation of atomically precise Au NCs. The design of an efficient synthesis of thiolated Au

* Address correspondence to chexiej@nus.edu.sg, cheleejy@nus.edu.sg.

Received for review May 25, 2012 and accepted August 22, 2012.

Published online August 22, 2012
10.1021/nn3023206

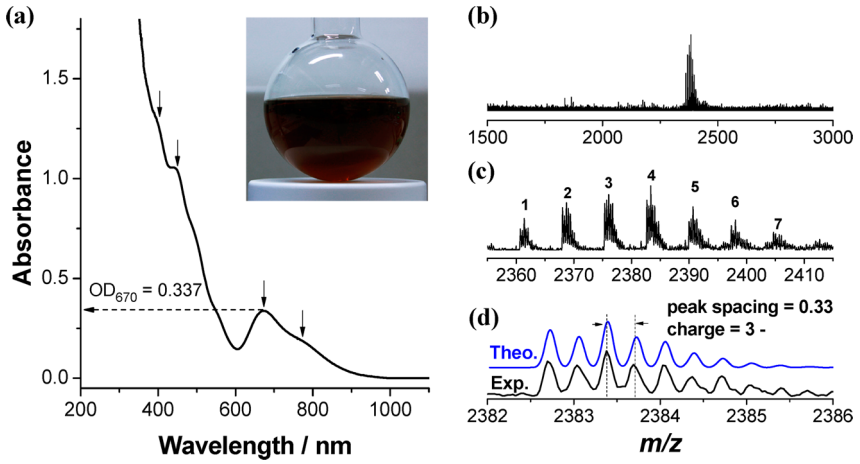

Figure 1. UV−vis spectrum (a) and ESI spectra (in negative ion mode; b−d) of the as-synthesized $Au_{25}(Cys)_{18}$ NCs. The blue curve in (d) is the theoretical isotope pattern of peak #4 in (c).

NCs needs a very detailed understanding of the NC growth process, which is presently lacking due to the use of strong reducing agents (*e.g.*, $NaBH_4$) in the NC synthesis. The very fast reduction kinetics therein makes it a challenge to follow the NC growth process (*e.g.*, size evolution), which can reveal important mechanistic insights.

Herein, we report a simple and versatile synthesis of thiolated Au NCs using a gaseous reducing agent, carbon monoxide (CO), to create a mild reduction environment for the Au ions. A large quantity of high-purity $Au_{25}(SR)_{18}$ NCs can be produced in a single batch by this one-pot method. The slow growth of $Au_{25}(SR)_{18}$ NCs in the presence of CO (~24 h) enabled the growth process to be followed for the first time (to the best of our knowledge) by UV−vis spectroscopy analysis of the reaction solution, which underwent distinct color changes (colorless → yellow → orange → brown → red-brown). Several key NC intermediates were identified by their characteristic UV−vis spectra and mass spectrometry analysis, thereby allowing the formation of $Au_{25}(SR)_{18}$ NCs to be reconstructed.

RESULTS AND DISCUSSION

The Au NCs were protected by cysteine (Cys), a common amino acid selected as the model thiol ligand for this study. In a typical synthesis of $Au_{25}(Cys)_{18}$ NCs, an aqueous $HAuCl_4$ solution (3.75 mL, 40 mM; or 60 mg of $HAuCl_4 \cdot 3H_2O$) and a Cys solution (4.5 mL, 50 mM, pH = 12; or 27 mg of Cys) were added to ultrapure water (141.75 mL) under vigorous stirring, followed by NaOH addition to bring the pH of the reaction mixture to 11. The reaction vessel was then saturated with 1 bar CO for 2 min. The reaction mixture was sealed airtight, and the reaction was allowed to proceed under gentle stirring (500 rpm) at room temperature for 24 h. The color of the solution changed from colorless to yellow, orange, brown, and finally red-brown (Figure 1a, inset).

Raw product was collected after 24 h of reaction and examined by UV−vis spectroscopy. The resulting spectrum (Figure 1a) shows four distinct absorption peaks at 400, 450, 670, and 770 nm, which are the characteristic absorption of thiolated Au_{25} NCs.[23,37] The well-defined absorption spectrum suggests high-purity $Au_{25}(Cys)_{18}$ NCs in the raw product. A very high yield of $Au_{25}(Cys)_{18}$ NCs (~95% based on the amount of Au in the precursor) was determined by measuring the optical density of the raw product at 670 nm and using the reported molar absorption coefficient of thiolated Au_{25} NCs[14] (see Experimental Section for details).

ESI-MS was used to determine the molecular composition of the as-synthesized thiolated Au NCs. ESI is a soft ionization technique that allows the determination of the intact NC mass.[1,38,39] As shown in Figure 1b, only one set of intense peaks at *m/z* ~2380 is present in the range 1500−3000, further corroborating the high purity of the raw NCs. The base peak at *m/z* 2383.4 (#4, Figure 1c) is accompanied by a series of similar and less intense peaks (#1−#3, #5−#7) spaced 22 Da apart, which can be attributed to H^+ dissociation and Na^+ coordination [$-H + Na$].[40] The isotope pattern analysis (Figure 1d, blue (theoretical) and black (experimental) curve) of the 2383.4 peak (#4) indicates that the ionized NCs carried three negative charges (isotopic peak spacing = 0.33). Thus the molecular weight of the NCs could be determined as 7150.2 Da (2383.4 × 3), consistent with the molecular formula of $[Au_{25}(Cys)_{18} - 6H + 3Na]^{3-}$ (molecular weight of 7150.0 Da). Other identifiable ionized species in the set include $[Au_{25}(Cys)_{18} - 3H]^{3-}$ (7083.2 Da, #1), $[Au_{25}(Cys)_{18} - 4H + Na]^{3-}$ (7106.1 Da, #2), $[Au_{25}(Cys)_{18} - 5H + 2Na]^{3-}$ (7128.1 Da, #3), $[Au_{25}(Cys)_{18} - 7H + 4Na]^{3-}$ (7193.1 Da, #5), $[Au_{25}(Cys)_{18} - 8H + 5Na]^{3-}$(7194.1 Da, #6), and $[Au_{25}(Cys)_{18} - 9H + 6Na]^{3-}$ (7216.2 Da, #7) (see Figure S1 for their respective isotope patterns).

Matrix-assisted laser desorption ionization time-of-flight (MALDI-TOF) spectrometry was also used to

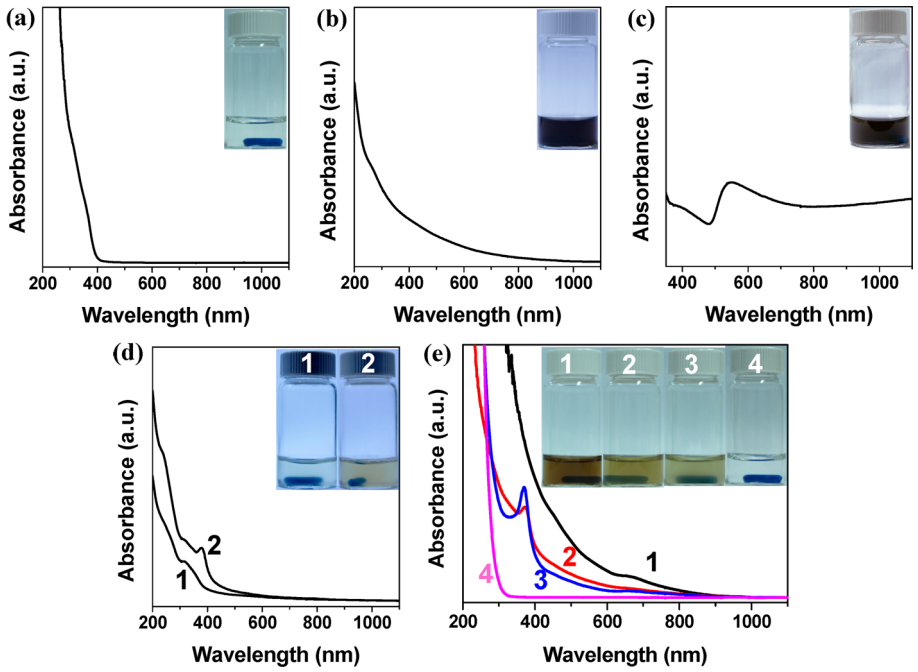

Figure 2. UV−vis spectra and digital photographs (inset) of (a) the mixture of $HAuCl_4$ and Cys in the absence of CO after 24 h of reaction (pH = 11); (b) Au NCs synthesized by substitution of CO with $NaBH_4$; (c) Au nanoparticles synthesized by the CO reduction without Cys; (d) Au NCs synthesized under different pHs (pH 4.4 (no. 1) and pH 9.1 (no. 2)); and (e) Au NCs synthesized by different $R_{[Cys]/[Au]}$ values at pH 11 ($R_{[Cys]/[Au]}$ = 1 (no. 1), $R_{[Cys]/[Au]}$ = 2 (no. 2), $R_{[Cys]/[Au]}$ = 3 (no. 3), and $R_{[Cys]/[Au]}$ = 4 (no. 4)).

confirm the NC formulas. MALDI-TOF is another technique for determining the NC composition. Extensive fragmentations could occur during analysis but could be suppressed by optimizing the operating conditions (*e.g.,* a proper selection of matrix and laser pulse intensity).[32,41] The peak at *m/z* ~7200 (Figure S2, in negative ion mode) corresponds well with the molecular formula $Au_{25}(Cys)_{18}$. The two smaller peaks at approximately *m/z* 5900 and 6700 can be assigned to $Au_{21}(Cys)_{14}$ and $Au_{24}(Cys)_{16}$, which are the residues of $Au_{25}(Cys)_{18}$ clusters after the common dissociation of a $Au_4(Cys)_4$ and a $Au(Cys)_2$ fragment, respectively.[41,42] No other peaks are found in the mass range up to *m/z* 15000, which is not unexpected in view of the high purity of the product. A representative transmission electron microscopy (TEM) image confirms that the NCs were highly monodisperse (Figure S3). The oxidation state of $Au_{25}(Cys)_{18}$ was determined by X-ray photoelectron spectroscopy (XPS). The Au $4f_{7/2}$ binding energy of the as-synthesized NCs (Figure S4a, black curve) is between that of thiolated-Au(I) complexes (prepared by simply mixing $HAuCl_4$ with Cys ligands, Figure S4a, red curve) and large Au nanoparticles (>3 nm, prepared by the $NaBH_4$ reduction of $HAuCl_4$ without any protecting agent, Figure S4a, blue curve). A slight 0.36 eV shift in the Au $4f_{7/2}$ binding energy from that of large Au nanoparticles may be attributed to the effects of surface thiolates.[14] The binding energy of S 2p at 163 eV (Figure S4b) is typical of the binding energy of thiolates in thiolated Au NCs.[35,43]

Several critical experimental conditions for the formation of high-purity $Au_{25}(Cys)_{18}$ NCs were identified: (i) Use of CO and Cys to provide, respectively, a mild reduction environment and strong protection is indispensable for the synthesis of high-purity $Au_{25}(Cys)_{18}$ NCs. CO is a mild reducing agent,[44−46] which reduced the precursor Au ions to Au metal, without which only thiolate-Au(I) complexes (Figure 2a) were formed at room temperature. It should be mentioned that Cys is also a weak reducing agent for the Au(III) ions.[47] However it could only reduce the Au(III) ions to Cys-Au(I) complexes under the prevailing reaction conditions at room temperature, as shown in Figure 2a. The strong affinity of thiol for Au(I) in the thiolate-Au(I) complexes protected the Au(I) oxidation state from further reduction by a weak reducing agent (Cys) under a mild reaction condition. On the other hand, substitution of CO with a stronger reducing agent ($NaBH_4$) produced a mixture of Au NCs in different sizes (and consequently a featureless absorption spectrum, see Figure 2b), thus highlighting the key role of CO in the synthesis. The unique thiolate-Au interactions are absolutely essential for the formation of ultrafine Au NCs. In the absence of the thiol ligands (Cys), only large Au nanoparticles with characteristic surface plasmon resonance (SPR) at ~540 nm (Figure 2c) were formed. (ii) A high pH (~11) of the reaction solution was necessary for the formation of $Au_{25}(Cys)_{18}$ NCs. A lower alkalinity (pH ≈ 9) or acidic (pH ≈ 4) condition would form Au NCs in other sizes (Figure 2d). The pH of the reaction solution could affect the formation of Cys-protected Au

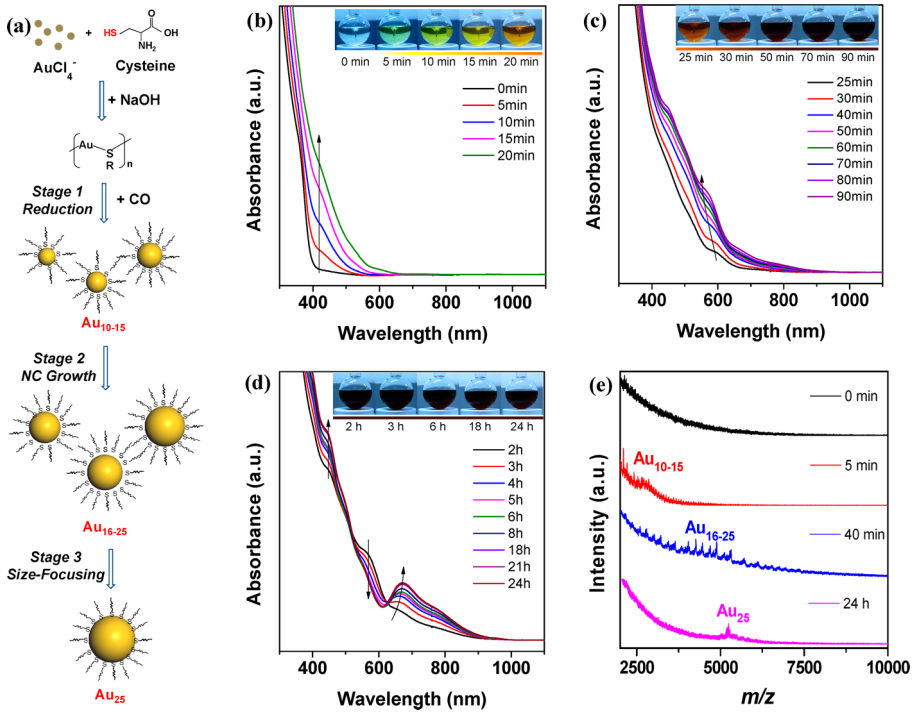

Figure 3. (a) Schematic diagram illustrating the postulated formation of $Au_{25}(Cys)_{18}$ NCs in the presence of CO. UV−vis spectra as a function of reaction time: (b) 0−20 min; (c) 20−90 min; and (d) 90 min to 24 h. Insets are digital photographs of the reaction solution at different times. (e) MALDI-TOF mass spectra (in positive ion mode) of the reaction solution at different reaction times: 0 min (black), 5 min (red), 40 min (blue), and 24 h (magenta).

NCs in two different ways. First, other than the thiol side group, which interacted with Au(I) to form Cys-Au(I) complexes, Cys has two other ionizable functional groups (carboxyl and amine, resulting in two pK_a values of 1.71 and 10.78, respectively).[48] Therefore the solution pH determined the ionization of the Cys ligand and consequently the formation of different Cys-Au(I) complexes or different aggregation state of the Cys-Au(I) complexes, to result in different rates of formation of the Au NCs, similar to the observations in previous studies.[29,49] Second, the reduction capability of CO is also pH dependent. Increase of the reaction pH in our reaction system increased the reduction capability of CO because the product of CO oxidation—CO_2—was more soluble in water as CO_3^{2-}.

(iii) The monodispersity of the $Au_{25}(Cys)_{18}$ NCs was dependent on the ligand (Cys) to Au precursor concentration ratio ($R_{[Cys]/[Au]}$). Other studies have found this ratio to be determining of the size of the Au NC product.[50] Different $R_{[Cys]/[Au]}$ ratios (1, 1.5, 2, 3, and 4) were also used in our synthesis, and the most optimal ratio for the $Au_{25}(Cys)_{18}$ NCs was 1.5 (Figure 1). A lower ($R_{[Cys]/[Au]}$ = 1, Figure 2e, no. 1) or higher ($R_{[Cys]/[Au]}$ = 2 or 3, Figure 2e, no. 2 and no. 3, respectively) ratio would produce Au NCs in other sizes, as shown by their respective optical absorption spectra (Figure 2e). It should be noted that when the ligand to Au ratio was increased to 4, only a colorless solution (Figure 2e, no. 4) with no absorption peaks in the wavelength range of 300 to 1100 nm was obtained, suggesting the formation of ultrasmall Au NCs.

Slow and controllable reaction kinetics is another noticeable feature of the CO-directed synthesis of $Au_{25}(Cys)_{18}$ NCs. NC formation occurred through a series of distinct color changes that could be followed by the time-course measurements of the UV−vis spectra. The NC size was found to vary from Au_{10-15}, to Au_{16-25}, and finally to Au_{25} based on UV−vis spectroscopy and mass spectrometry measurements. A postulation of the growth of thiolated Au_{25} NCs in the presence of CO is illustrated in Figure 3a. This particular scheme identifies three distinguishable stages: the formation of Au_{10-15} NCs from thiolate-Au(I) complexes *via* CO reduction (stage 1), the NC growth from Au_{10-15} to Au_{16-25} NCs (stage 2), and the transformation (or size-focusing) of Au_{16-25} to the final Au_{25} NCs (stage 3).

The first stage was the formation of Au_{10-15} NCs by the CO reduction of thiolate-Au(I) complexes. The initially colorless solution was instantaneously changed to light yellow after the introduction of CO. The solution color deepened gradually to yellow and was orange in 20 min (Figure 3b, inset). The light yellow solution after 5 min of reaction displayed a shoulder peak at ~420 nm, which grew in intensity with time (Figure 3b). The absorption peak at ~420 nm is close to the characteristic absorptions of the reported Au_{10-15} NCs, which are in the wavelength range of 370 to 420 nm.[14,51−53] The formation of Au_{10-15} NC intermediates was confirmed by the MALDI-TOF analysis of the solution after 5 min of reaction. The bump in the

spectrum at m/z ~2600 (Figure 3e, red curve; see also Figure S5a for the zoomed-in spectrum) suggests that the intermediate species after 5 min of reaction was in the size range of 10−15 Au atoms. Only the core mass of Au_nS_m was detected in our MALDI samples in the positive ion mode because of the significant fragmentation under the measurement conditions, similar to the observations in other studies.[20,54,55]

It should be mentioned that, besides serving as the reducing agent, CO could also be a surface protecting ligand in the Au NC synthesis. The strong affinity of CO for the noble metal surface[56−58] is well known and could be involved in the stabilization of Au_{10-15} NC intermediates formed in the early stages of the reaction. However, the CO molecules on the surface of these small Au NC intermediates could be easily oxidized to CO_3^{2-} in alkaline solution due to the catalytic activity of small Au NCs for CO oxidation.[59,60] The loss of CO as a stabilizer destabilized the small Au NCs, facilitating the deposition of thiolate-Au(I) motifs for surface protection and the subsequent growth of the Au NC intermediates into thiolated Au NCs. No CO was present in the final product ($Au_{25}(Cys)_{18}$ NCs), an indication of the completeness of CO oxidation catalyzed by the Au NC intermediates during synthesis.

The second stage was the growth of the NC intermediates from Au_{10-15} to Au_{16-25} NCs, as shown by the solution color change from orange to brown and finally to red-brown after 20 to 90 min of reaction (Figure 3c, inset). A prominent peak at ~590 nm appeared after 25 min of reaction (Figure 3c). The ~590 nm peak gradually shifted to lower wavelengths with time and was at ~560 nm after 90 min of reaction. This peak is in the range of the characteristic absorptions of the reported Au_{16-25} NCs (~540−570 nm).[14] MALDI-TOF mass spectrometry analyses attested to the formation of Au_{16-25} NC intermediates in the reaction solution in stage 2. For instance, the MALDI-TOF mass spectrum of the reaction solution at 40 min (Figure 3e, blue curve, and Figure S5b for the zoomed-in spectrum) implicated Au NC species in a size range of 16−25 Au atoms.

The third stage was the transformation (or size-focusing) of Au_{16-25} NC intermediates to Au_{25} NCs. This commenced after 90 min of reaction when the color of the reaction solution stayed at red-brown with no further changes detectable by the naked eye (Figure 3d, inset). After 2 h of reaction, a peak at ~640 nm was highly visible in the UV−vis spectrum (Figure 3d). The peak location is close to the characteristic absorption of Au_{25} NCs at 670 nm. The peak gradually shifted to longer wavelengths and stabilized at 670 nm at about 8 h of reaction, whereas the intensity increased with time from 8 to 18 h. At the same time other fingerprint peaks of Au_{25} NCs at 400, 450, and 770 nm also emerged and increased in intensity with time. A complete absorption profile of

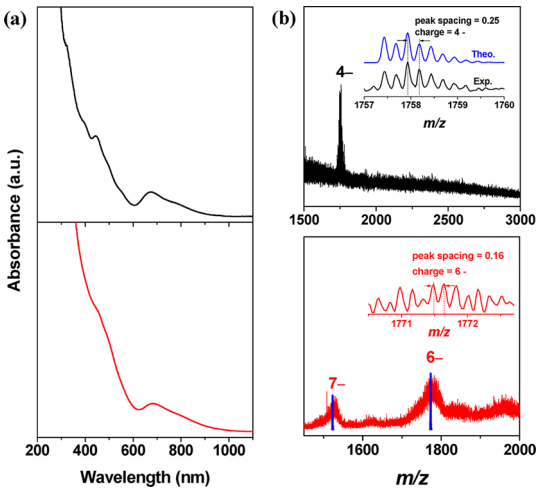

Figure 4. UV−vis spectra (a) and ESI mass spectra (in negative ion mode; b) of $Au_{25}(SR)_{18}$ NCs synthesized by using MPA (black curve) and GSH (red curve) as the protecting agent. The inset in the top panel of (b) is the experimental (black curve) and theoretical (blue curve) isotope pattern of the most abundant species in MPA-Au_{25} NCs ($[Au_{25}(MPA)_{18} - 14H + 10Na]^{4-}$). The inset in the bottom panel of (b) is the isotope pattern analysis of the 6− ion in GSH-Au_{25} NCs, and the blue curves are the predicted isotope distributions of the two most abundant species ($[Au_{25}(GSH)_{18} - 17H + 10Na]^{7-}$ and $[Au_{25}(GSH)_{18} - 15H + 9Na]^{6-}$).

Au_{25} NCs was fully developed in about 18 h. The intensity increase of the 670 nm peak correlated well with the decrease of the 560 nm peak, thereby suggesting the size-focusing of Au_{16-25} NCs to Au_{25} NCs. The presence of only one intense peak corresponding to the Au_{25} NCs in the MALDI-TOF spectrum (Figure 3e, magenta curve) of the reaction solution at 24 h is further indication of the size-focusing of Au_{16-25} to Au_{25} NCs in stage 3. Although the details on the size-focusing of Au_{16-25} NCs to Au_{25} NCs are not clear at this time, it could be thermodynamically driven; it has been reported that Au_{25} NCs are thermodynamically more stable than other NC species in the size range of Au_{16} to Au_{25}.[22] The absorption spectrum of the reaction solution was practically unchanged from 18 to 24 h. This was also the time period our final product was sampled.

The synthesis protocol developed in this study is easily scalable (*e.g.*, to 1 L, or ~200 mg of $Au_{25}(Cys)_{18}$ NCs in a single batch, Figure S6). It is also fairly generic and can be easily adapted to synthesize Au_{25} NCs protected by other thiol ligands, such as 3-mercaptopropionic acid (MPA) and glutathione (GSH). For example, Figure 4a shows the absorption spectra of Au NCs synthesized by using CO as the reducing agent and MPA or GSH as the protecting agent. The absorption spectra of MPA- (black curve) and GSH-protected (red curve) Au_{25} NCs are nearly identical to that of Cys-protected Au_{25} NCs (Figure 1a). The corresponding molecular formulas were determined to be $Au_{25}(MPA)_{18}$ and $Au_{25}(GSH)_{18}$, respectively (Figure 4b).

CONCLUSION

In summary, we have developed a simple one-pot method for the synthesis of high-purity thiolated $Au_{25}(Cys)_{18}$ NCs (~95% yield) by using gaseous CO as a mild reducing agent. The preparation can be easily scaled up for large-scale production and for producing atomically precise Au NCs protected by other thiol ligands. Distinct color changes were observed for the first time during the formation of thiolated Au_{25} NCs, and several key intermediates in the growth of $Au_{25}(Cys)_{18}$ NCs (NCs of Au_{10-15}, Au_{16-25}, and Au_{25}) could be identified from the time course measurements of UV–vis spectroscopy and MALDI-TOF data. The formation of $Au_{25}(Cys)_{18}$ NCs was found to proceed through three identifiable stages: the reduction of thiolate-Au(I) complexes to Au_{10-15} NCs (stage 1), the NC growth of Au_{10-15} into Au_{16-25} NCs (stage 2), and the transformation or size-focusing of Au_{16-25} NCs to Au_{25} NCs (stage 3). This method of preparation is of interest not only because it provides a simple one-pot procedure for the preparation of thiolated Au_{25} NCs, but also because it demonstrates the unique reaction environment provided by gaseous CO. It opens up a new synthesis route for the fabrication of atomically precise metal (Au, Ag, Pt, and Cu) NCs in quantities large enough for application explorations.

EXPERIMENTAL SECTION

Chemicals. Hydrogen tetrachloroaurate(III) hydrate ($HAuCl_4 \cdot 3H_2O$) was purchased from Alfa Aesar. L-Cysteine (Cys), L-glutathione reduced (GSH), and 3-mercaptopropionic acid (MPA) were purchased from Sigma-Aldrich. Carbon monoxide (99.9%) was supplied by Singapore Oxygen Air Liquide Pte Ltd. (SOXAL). All chemicals were used as received. All glassware were washed with Aqua Regia (HCl:HNO_3 volume ratio = 3:1) and rinsed with ethanol and ultrapure water. Ultrapure water with a specific resistance of 18.2 MΩ was used throughout the experiment.

Synthesis of $Au_{25}(Cys)_{18}$ NCs. In a typical synthesis, aqueous $HAuCl_4$ solution (3.75 mL, 40 mM; or 60 mg of $HAuCl_4 \cdot 3H_2O$) and Cys solution (4.5 mL, 50 mM, pH = 12; or 27 mg of Cys) were added to ultrapure water (141.75 mL) under vigorous stirring, followed by NaOH addition to adjust the pH of the reaction solution to 11. The reaction vessel was then saturated with 1 bar CO for 2 min. The reaction mixture was sealed airtight, and the reaction was allowed to proceed under gentle stirring (500 rpm) at room temperature for 24 h. The time CO was introduced to the reaction solution was recorded as 0 min. At specific time intervals, small aliquots of the reaction solution were drawn with a syringe (1 mL) and analyzed by UV–vis spectroscopy. The final product was collected at 24 h, followed by concentration in a rotary evaporator. The thiolated Au NCs were then precipitated out by adding an adequate amount of ethanol. The precipitate was collected, washed with methanol several times, and vacuum-dried. For a typical synthesis, ~40 mg of $Au_{25}(Cys)_{18}$ NCs was obtained. About 200 mg of $Au_{25}(Cys)_{18}$ NCs could be obtained from a large-scale synthesis. The synthesis of Au_{25} NCs protected by other thiol ligands (MPA and GSH) was carried out under similar conditions except for the replacement of Cys by other thiol ligands.

Materials Characterizations. UV–vis spectra were recorded on a Shimadzu UV-1800 spectrometer. The molecular formulas of Au NCs were analyzed by a Bruker MicroTOF-Q electrospray ionization time-of-flight (ESI-TOF) system operating in the negative ion mode (capillary voltage: 4 kV; nebulizer: 0.4 bar; dry gas: 2 L·min^{-1} at 120 °C; *m/z*: 50–4000). Samples were dissolved in ultrapure water and injected into the chamber at 120 μL·min^{-1}. The matrix-assisted laser desorption ionization time-of-flight (MALDI-TOF) mass spectra of Au NCs were recorded by a Bruker Daltonics Autoflex II TOF/TOF system. The MALDI-TOF samples were prepared by mixing 2 μL of the raw product with 2 μL of matrix solution (saturated α-cyano-4-hydroxycinnamic acid (CHCA) solution in 50% acetonitrile) and allowed for recrystallization in air prior to the analysis. The data were collected in linear mode (negative ion or positive ion). Transmission electron microscopy (TEM) images were taken on a JEOL JEM-2010 microscope operating at 200 kV. X-ray photoelectron spectroscopy measurements were performed on a VG ESCALAB MKII spectrometer.

Estimation of the Yield of $Au_{25}(Cys)_{18}$ NCs. $Au_{25}(SR)_{18}$ NCs of nearly 100% purity were recovered by PAGE separation. The optical density at 670 nm of our raw product was 0.337 (Figure 1a). Using a molar absorption coefficient (ε) at 670 nm of 8.8×10^3 M^{-1}·cm^{-1},[14] the concentration of $Au_{25}(SR)_{18}$ in the raw product was calculated to be 3.8×10^{-2} mM. Since the initial Au ion concentration in our reaction solution was 1 mM, the yield of $Au_{25}(SR)_{18}$ in our raw product based on the total amount of Au precursor ions in the reaction solution was therefore ~95% $\{(3.8 \times 10^{-2} \times 25\ \text{mM})/1\ \text{mM} = 95\%\}$.

Conflict of Interest: The authors declare no competing financial interest.

Acknowledgment. This work is financially supported by the Ministry of Education, Singapore, under Grants R-279-000-295-133 and R-279-000-327-112. Yong Yu acknowledges the National University of Singapore for his research scholarship.

Supporting Information Available: Figure S1, isotope patterns of peaks #1–#3 and #5–#7 in Figure 1c; Figure S2–S4, MALDI-TOF mass spectrum in negative ion mode, TEM, and XPS analysis of the as-synthesized Au_{25} NCs protected by cysteine; Figure S5, zoomed-in MALDI-TOF mass spectra for the reaction solution at (a) 5 min and (b) 40 min; Figure S6, characterizations of the as-synthesized $Au_{25}(Cys)_{18}$ NCs in a 2 L flask. This material is available free of charge *via* the Internet at http://pubs.acs.org.

REFERENCES AND NOTES

1. Jin, R. Quantum Sized, Thiolate-Protected Gold Nanoclusters. *Nanoscale* **2010**, *2*, 343–362.
2. Zhang, Q.; Xie, J.; Yu, Y.; Lee, J. Y. Monodispersity Control in the Synthesis of Monometallic and Bimetallic Quasi-Spherical Gold and Silver Nanoparticles. *Nanoscale* **2010**, *2*, 1962–1975.
3. Chen, S.; Ingram, R. S.; Hostetler, M. J.; Pietron, J. J.; Murray, R. W.; Schaaff, T. G.; Khoury, J. T.; Alvarez, M. M.; Whetten, R. L. Gold Nanoelectrodes of Varied Size: Transition to Molecule-Like Charging. *Science* **1998**, *280*, 2098–2101.
4. Murray, R. W. Nanoelectrochemistry: Metal Nanoparticles, Nanoelectrodes, and Nanopores. *Chem. Rev.* **2008**, *108*, 2688–2720.
5. Laaksonen, T.; Ruiz, V.; Liljeroth, P.; Quinn, B. M. Quantised Charging of Monolayer-Protected Nanoparticles. *Chem. Soc. Rev.* **2008**, *37*, 1836–1846.
6. Shang, L.; Dong, S.; Nienhaus, G. U. Ultra-Small Fluorescent Metal Nanoclusters: Synthesis and Biological Applications. *Nano Today* **2011**, *6*, 401–418.
7. Yuan, X.; Luo, Z.; Zhang, Q.; Zhang, X.; Zheng, Y.; Lee, J. Y.; Xie, J. Synthesis of Highly Fluorescent Metal (Ag, Au, Pt, and Cu) Nanoclusters by Electrostatically Induced Reversible Phase Transfer. *ACS Nano* **2011**, *5*, 8800–8808.
8. Xie, J.; Zheng, Y.; Ying, J. Y. Protein-Directed Synthesis of Highly Fluorescent Gold Nanoclusters. *J. Am. Chem. Soc.* **2009**, *131*, 888–889.

9. Zhou, C.; Sun, C.; Yu, M.; Qin, Y.; Wang, J.; Kim, M.; Zheng, J. Luminescent Gold Nanoparticles with Mixed Valence States Generated from Dissociation of Polymeric Au(I) Thiolates. *J. Phys. Chem. C* **2010**, *114*, 7727–7732.
10. Zheng, J.; Nicovich, P. R.; Dickson, R. M. Highly Fluorescent Noble-Metal Quantum Dots. *Annu. Rev. Phys. Chem.* **2007**, *58*, 409–431.
11. Zhu, Y.; Qian, H.; Zhu, M.; Jin, R. Thiolate-Protected Au_n Nanoclusters as Catalysts for Selective Oxidation and Hydrogenation Processes. *Adv. Mater.* **2010**, *22*, 1915–1920.
12. Zhu, Y.; Qian, H.; Jin, R. An Atomic-Level Strategy for Unraveling Gold Nanocatalysis from the Perspective of $Au_n(SR)_m$ Nanoclusters. *Chem.—Eur. J.* **2010**, *16*, 11455–11462.
13. Liu, Y.; Tsunoyama, H.; Akita, T.; Xie, S.; Tsukuda, T. Aerobic Oxidation of Cyclohexane Catalyzed by Size-Controlled Au Clusters on Hydroxyapatite: Size Effect in the Sub-2 nm Regime. *ACS Catal.* **2010**, *1*, 2–6.
14. Negishi, Y.; Nobusada, K.; Tsukuda, T. Glutathione-Protected Gold Clusters Revisited: Bridging the Gap between Gold(I)−Thiolate Complexes and Thiolate-Protected Gold Nanocrystals. *J. Am. Chem. Soc.* **2005**, *127*, 5261–5270.
15. Brust, M.; Walker, M.; Bethell, D.; Schiffrin, D. J.; Whyman, R. Synthesis of Thiol-Derivatised Gold Nanoparticles in a Two-Phase Liquid-Liquid System. *J. Chem. Soc., Chem. Commun.* **1994**, 801–802.
16. Daniel, M.-C.; Astruc, D. Gold Nanoparticles: Assembly, Supramolecular Chemistry, Quantum-Size-Related Properties, and Applications toward Biology, Catalysis, and Nanotechnology. *Chem. Rev.* **2003**, *104*, 293–346.
17. Goulet, P. J. G.; Lennox, R. B. New Insights into Brust−Schiffrin Metal Nanoparticle Synthesis. *J. Am. Chem. Soc.* **2010**, *132*, 9582–9584.
18. Schaaff, T. G.; Shafigullin, M. N.; Khoury, J. T.; Vezmar, I.; Whetten, R. L.; Cullen, W. G.; First, P. N.; Gutiérrez-Wing, C.; Ascensio, J.; Jose-Yacamán, M. J. Isolation of Smaller Nanocrystal Au Molecules: Robust Quantum Effects in Optical Spectra. *J. Phys. Chem. B* **1997**, *101*, 7885–7891.
19. Schaaff, T. G.; Whetten, R. L. Giant Gold−Glutathione Cluster Compounds: Intense Optical Activity in Metal-Based Transitions. *J. Phys. Chem. B* **2000**, *104*, 2630–2641.
20. Schaaff, T. G.; Knight, G.; Shafigullin, M. N.; Borkman, R. F.; Whetten, R. L. Isolation and Selected Properties of a 10.4 kDa Gold:Glutathione Cluster Compound. *J. Phys. Chem. B* **1998**, *102*, 10643–10646.
21. Murayama, H.; Narushima, T.; Negishi, Y.; Tsukuda, T. Structures and Stabilities of Alkanethiolate Monolayers on Palladium Clusters as Studied by Gel Permeation Chromatography. *J. Phys. Chem. B* **2004**, *108*, 3496–3503.
22. Shichibu, Y.; Negishi, Y.; Tsunoyama, H.; Kanehara, M.; Teranishi, T.; Tsukuda, T. Extremely High Stability of Glutathionate-Protected Au_{25} Clusters Against Core Etching. *Small* **2007**, *3*, 835–839.
23. Shichibu, Y.; Negishi, Y.; Tsukuda, T.; Teranishi, T. Large-Scale Synthesis of Thiolated Au_{25} Clusters *via* Ligand Exchange Reactions of Phosphine-Stabilized Au_{11} Clusters. *J. Am. Chem. Soc.* **2005**, *127*, 13464–13465.
24. Wu, Z.; Suhan, J.; Jin, R. One-Pot Synthesis of Atomically Monodisperse, Thiol-Functionalized Au_{25} Nanoclusters. *J. Mater. Chem.* **2009**, *19*, 622–626.
25. Heaven, M. W.; Dass, A.; White, P. S.; Holt, K. M.; Murray, R. W. Crystal Structure of the Gold Nanoparticle $[N(C_8H_{17})_4][Au_{25}(SCH_2CH_2Ph)_{18}]$. *J. Am. Chem. Soc.* **2008**, *130*, 3754–3755.
26. Zhu, M.; Aikens, C. M.; Hollander, F. J.; Schatz, G. C.; Jin, R. Correlating the Crystal Structure of a Thiol-Protected Au_{25} Cluster and Optical Properties. *J. Am. Chem. Soc.* **2008**, *130*, 5883–5885.
27. Toikkanen, O.; Ruiz, V.; Rönnholm, G.; Kalkkinen, N.; Liljeroth, P.; Quinn, B. M. Synthesis and Stability of Monolayer-Protected Au_{38} Clusters. *J. Am. Chem. Soc.* **2008**, *130*, 11049–11055.
28. Qian, H.; Zhu, Y.; Jin, R. Size-Focusing Synthesis, Optical and Electrochemical Properties of Monodisperse $Au_{38}(SC_2H_4Ph)_{24}$ Nanoclusters. *ACS Nano* **2009**, *3*, 3795–3803.
29. Qian, H.; Jin, R. Ambient Synthesis of $Au_{144}(SR)_{60}$ Nanoclusters in Methanol. *Chem. Mater.* **2011**, *23*, 2209–2217.
30. Chaki, N. K.; Negishi, Y.; Tsunoyama, H.; Shichibu, Y.; Tsukuda, T. Ubiquitous 8 and 29 kDa Gold:Alkanethiolate Cluster Compounds: Mass-Spectrometric Determination of Molecular Formulas and Structural Implications. *J. Am. Chem. Soc.* **2008**, *130*, 8608–8610.
31. Fields-Zinna, C. A.; Sardar, R.; Beasley, C. A.; Murray, R. W. Electrospray Ionization Mass Spectrometry of Intrinsically Cationized Nanoparticles, $[Au_{144/146}(SC_{11}H_{22}N(CH_2CH_3)^{3+})_x(S(CH_2)_5CH_3)_y]^{x+}$. *J. Am. Chem. Soc.* **2009**, *131*, 16266–16271.
32. Dharmaratne, A. C.; Krick, T.; Dass, A. Nanocluster Size Evolution Studied by Mass Spectrometry in Room Temperature $Au_{25}(SR)_{18}$ Synthesis. *J. Am. Chem. Soc.* **2009**, *131*, 13604–13605.
33. Zhu, M.; Qian, H.; Jin, R. Thiolate-Protected $Au_{24}(SC_2H_4Ph)_{20}$ Nanoclusters: Superatoms or Not? *J. Phys. Chem. Lett.* **2010**, *1*, 1003–1007.
34. Zhu, M.; Qian, H.; Jin, R. Thiolate-Protected Au_{20} Clusters with a Large Energy Gap of 2.1 eV. *J. Am. Chem. Soc.* **2009**, *131*, 7220–7221.
35. Wu, Z.; MacDonald, M. A.; Chen, J.; Zhang, P.; Jin, R. Kinetic Control and Thermodynamic Selection in the Synthesis of Atomically Precise Gold Nanoclusters. *J. Am. Chem. Soc.* **2011**, *133*, 9670–9673.
36. Schaaff, T. G.; Whetten, R. L. Controlled Etching of Au:SR Cluster Compounds. *J. Phys. Chem. B* **1999**, *103*, 9394–9396.
37. Parker, J. F.; Fields-Zinna, C. A.; Murray, R. W. The Story of a Monodisperse Gold Nanoparticle: $Au_{25}L_{18}$. *Acc. Chem. Res.* **2010**, *43*, 1289–1296.
38. Tracy, J. B.; Kalyuzhny, G.; Crowe, M. C.; Balasubramanian, R.; Choi, J.-P.; Murray, R. W. Poly(ethylene glycol) Ligands for High-Resolution Nanoparticle Mass Spectrometry. *J. Am. Chem. Soc.* **2007**, *129*, 6706–6707.
39. Tracy, J. B.; Crowe, M. C.; Parker, J. F.; Hampe, O.; Fields-Zinna, C. A.; Dass, A.; Murray, R. W. Electrospray Ionization Mass Spectrometry of Uniform and Mixed Monolayer Nanoparticles: $Au_{25}[S(CH_2)_2Ph]_{18}$ and $Au_{25}[S(CH_2)_2Ph]_{18-x}(SR)_x$. *J. Am. Chem. Soc.* **2007**, *129*, 16209–16215.
40. Wu, Z.; Lanni, E.; Chen, W.; Bier, M. E.; Ly, D.; Jin, R. High Yield, Large Scale Synthesis of Thiolate-Protected Ag_7 Clusters. *J. Am. Chem. Soc.* **2009**, *131*, 16672–16674.
41. Dass, A.; Stevenson, A.; Dubay, G. R.; Tracy, J. B.; Murray, R. W. Nanoparticle MALDI-Mass Spectrometry without Fragmentation: $Au_{25}(SCH_2CH_2Ph)_{18}$ and Mixed Monolayer $Au_{25}(SCH_2CH_2Ph)_{18-x}(L)_x$. *J. Am. Chem. Soc.* **2008**, *130*, 5940–5946.
42. Angel, L. A.; Majors, L. T.; Dharmaratne, A. C.; Dass, A. Ion Mobility Mass Spectrometry of $Au_{25}(SCH_2CH_2Ph)_{18}$ Nanoclusters. *ACS Nano* **2010**, *4*, 4691–4700.
43. Shibu, E. S.; Pradeep, T. Quantum Clusters in Cavities: Trapped Au_{15} in Cyclodextrins. *Chem. Mater.* **2011**, *23*, 989–999.
44. Pretzer, L. A.; Nguyen, Q. X.; Wong, M. S. Controlled Growth of Sub-10 nm Gold Nanoparticles Using Carbon Monoxide Reductant. *J. Phys. Chem. C* **2010**, *114*, 21226–21233.
45. Xie, J.; Zhang, Q.; Zhou, W.; Lee, J. Y.; Wang, D. I. C. Template-Free Synthesis of Porous Platinum Networks of Different Morphologies. *Langmuir* **2009**, *25*, 6454–6459.
46. Kang, Y.; Ye, X.; Murray, C. B. Size- and Shape-Selective Synthesis of Metal Nanocrystals and Nanowires Using CO as a Reducing Agent. *Angew. Chem., Int. Ed.* **2010**, *122*, 6292–6295.
47. Glisic, B. D.; Rychlewska, U.; Djuran, M. I. Reactions and Structural Characterization of Gold(III) Complexes with Amino Acids, Peptides and Proteins. *Dalton Trans.* **2012**, *41*, 6887–6901.
48. Dawson, R. M. C.; Elliott, D. C.; Elliott, W. H. *Data for Biochemical Research*; Clarendon Press: Oxford, 1989.
49. Zhu, M.; Lanni, E.; Garg, N.; Bier, M. E.; Jin, R. Kinetically Controlled, High-Yield Synthesis of Au_{25} Clusters. *J. Am. Chem. Soc.* **2008**, *130*, 1138–1139.
50. Negishi, Y.; Sakamoto, C.; Ohyama, T.; Tsukuda, T. Synthesis and the Origin of the Stability of Thiolate-Protected Au_{130} and Au_{187} Clusters. *J. Phys. Chem. Lett.* **2012**, *3*, 1624–1628.

51. Woehrle, G. H.; Warner, M. G.; Hutchison, J. E. Ligand Exchange Reactions Yield Subnanometer, Thiol-Stabilized Gold Particles with Defined Optical Transitions. *J. Phys. Chem. B* **2002**, *106*, 9979–9981.
52. Yang, Y.; Chen, S. Surface Manipulation of the Electronic Energy of Subnanometer-Sized Gold Clusters: An Electrochemical and Spectroscopic Investigation. *Nano Lett.* **2002**, *3*, 75–79.
53. Bertino, M. F.; Sun, Z.-M.; Zhang, R.; Wang, L.-S. Facile Syntheses of Monodisperse Ultrasmall Au Clusters. *J. Phys. Chem. B* **2006**, *110*, 21416–21418.
54. Wu, Z.; Gayathri, C.; Gil, R. R.; Jin, R. Probing the Structure and Charge State of Glutathione-Capped $Au_{25}(SG)_{18}$ Clusters by NMR and Mass Spectrometry. *J. Am. Chem. Soc.* **2009**, *131*, 6535–6542.
55. Yang, X.; Su, Y.; Paau, M. C.; Choi, M. M. F. Mass Spectrometric Identification of Water-Soluble Gold Nanocluster Fractions from Sequential Size-Selective Precipitation. *Anal. Chem.* **2012**, *84*, 1765–1771.
56. Chang, S.-H.; Yeh, M.-H.; Pan, C.-J.; Chen, K.-J.; Ishii, H.; Liu, D.-G.; Lee, J.-F.; Liu, C.-C.; Rick, J.; Cheng, M.-Y.; Hwang, B.-J. CO-Assisted Synthesis of Finely Size-Controlled Platinum Nanoparticles. *Chem. Commun.* **2011**, *47*, 3864–3866.
57. Wu, B.; Zheng, N.; Fu, G. Small Molecules Control the Formation of Pt Nanocrystals: A Key Role of Carbon Monoxide in the Synthesis of Pt Nanocubes. *Chem. Commun.* **2011**, *47*, 1039–1041.
58. Wu, J.; Gross, A.; Yang, H. Shape and Composition-Controlled Platinum Alloy Nanocrystals Using Carbon Monoxide as Reducing Agent. *Nano Lett.* **2011**, *11*, 798–802.
59. Maye, M. M.; Lou, Y.; Zhong, C.-J. Core−Shell Gold Nanoparticle Assembly as Novel Electrocatalyst of CO Oxidation. *Langmuir* **2000**, *16*, 7520–7523.
60. Herzing, A. A.; Kiely, C. J.; Carley, A. F.; Landon, P.; Hutchings, G. J. Identification of Active Gold Nanoclusters on Iron Oxide Supports for CO Oxidation. *Science* **2008**, *321*, 1331–1335.